ADVANCED FUNCTIONAL MATERIALS
www.afm-journal.de

Self-Powered Intelligent Buoy Based on Triboelectric Nanogenerator for Water Level Alarming

Xi Liang, Shijie Liu, Zewei Ren, Tao Jiang, and Zhong Lin Wang**

With increasing global warming, catastrophic floods have threatened people's lives seriously and caused huge economic losses. However, present water hazard alarming systems generally rely on commercial batteries, limiting the intelligent development of disaster prevention planning and maintenance costs. In order to break the limitation, this work applies triboelectric nanogenerators (TENGs) to water hazard alarming. A spherical TENG device with four spiral units is designed to harvest water wave energy, and charge excitation modules (CEMs) are created and integrated with the TENG to improve its electric output. The output current and output power of the spherical TENG with CEMs can reach 15.09 mA and 24.48 mW, which are increased by 250.5 and 4.0 times, compared to the TENG without CEMs. Based on the charge excitation TENG, a self-powered intelligent buoy is constructed. Utilizing the buoy to transmit 433 MHz radio frequency signals to 25 meters away, a water level alarm system and a water level information exchange system with a mobile phone are successfully realized. This work extends applications of TENGs toward water wave energy harvesting and provides a new strategy for water hazard alarming, which is conducive to the fields of carbon neutralization, Internet of Things, and disaster prevention.

1. Introduction

Damaging floods are increasing in severity, duration, and frequency, owing to changes in climate, land use, infrastructure, and population demographics.[1,2] The global economic loss caused by flood damages occurred from 2000 to 2019 is estimated to be US$ 651 billion.[1,3] Under the urgent demands of the times, it is of great economic value and social significance to explore scientific and advanced water hazard risk management solutions.[4–6] Due to the suddenness and randomness of extreme weather and the complicated mechanism of floods,[2] water hazard alarming systems must have the ability to detect hydrological data promptly to achieve reliable water hazard response. However, present water hazard alarming systems generally rely on batteries, but the battery capacities are finite and their maintenance and replacement are difficult. Therefore, exploiting new power supply methods for water hazard alarming systems is the key to realizing timely and efficient water hazard alarming.

Triboelectric nanogenerator (TENG, also called as Wang generator) was invented in 2012 as an advanced technology for converting ambient mechanical energy to electrical energy,[7] which is the application of Maxwell's displacement current in energy and sensors.[8,9] Compared with traditional energy harvesting technologies, TENGs have a series of advantages such as simple mechanism,[10] lightweight,[11] high power density,[12–14] and low-frequency adaptation,[15–17] exhibiting great application potentials in many fields.[9,18–20] Among them, utilizing TENGs to harvest water wave energy is one of the most promising directions.[21–24] So far, the development of TENGs toward water wave energy harvesting not only alleviates the serious energy crisis, but also provides an effective solution for the distributed energy demand of the Internet of Things (IoTs).[25–30] Several studies have been carried out regarding a series of designs and explorations on the detection and wireless transmission of hydrological information based on TENGs.[31–35] However, because of the relatively low output performance of TENGs driven by the water wave motions, their function applications are still limited, and there is some distance away from real industrialization. Therefore, it is of great significance to propose the schemes of output performance improvement for TENGs and expand the application range.

X. Liang, S. Liu, T. Jiang, Z. L. Wang
CAS Center for Excellence in Nanoscience
Beijing Key Laboratory of Micro-nano Energy and Sensor
Beijing Institute of Nanoenergy and Nanosystems
Chinese Academy of Sciences
Beijing 101400, P. R. China
E-mail: jiangtao@binn.cas.cn; zhong.wang@mse.gatech.edu

X. Liang, S. Liu, T. Jiang, Z. L. Wang
School of Nanoscience and Technology
University of Chinese Academy of Sciences
Beijing 100049, P. R. China

Z. Ren
School of Advanced Materials and Nanotechnology
Academy of Advanced Interdisciplinary Research
Xidian University
Xi'an 710126, P. R. China

Z. L. Wang
School of Materials Science and Engineering
Georgia Institute of Technology
Atlanta, GA 30332-0245, USA

The ORCID identification number(s) for the author(s) of this article can be found under https://doi.org/10.1002/adfm.202205313.

DOI: 10.1002/adfm.202205313

In this work, we combined the exploitation of TENGs for water wave energy harvesting and the development of water hazard alarming systems through fabricating a self-powered intelligent buoy based on the TENG. First, for the wave conditions of the water hazard environment, we designed and fabricated a spherical TENG device loaded with four spiral TENG units, which were arranged as a regular tetrahedron. Then, a new charge excitation module (CEM) was devised and integrated with the TENG to further improve its output performance. With the CEM, the output current of a spiral TENG unit was elevated from 4.0 μA to 4.3 mA, and the corresponding transferred charge was enhanced from 38.5 nC to 2.9 μC. On the basis of structural optimization, the spherical TENG integrated with CEMs was placed in various water wave conditions and the output characteristics were systematically measured. Finally, a self-powered intelligent buoy was constructed by connecting the spherical TENG, the CEMs, and the function circuits together. Utilizing the self-powered intelligent buoy, a water level alarm system and a water level information exchange system with a mobile phone were demonstrated. This work not only expands the applications of TENGs to the field of water hazard prevention, but also proves its development potential for the IoTs.

2. Results and Discussion

The schematic illustration of a self-powered water hazard alarming system using an intelligent TENG-based buoy through water wave energy harvesting is shown in **Figure 1**a. The framework of the self-powered intelligent buoy for water level alarming is systematically depicted in Figure 1b. The self-powered intelligent buoy mainly contains three parts: the TENG, the CEM, and the sensing and signal transmitting unit. The TENG was utilized to harvest water wave energy in the working environment, converting the mechanical energy to the electrical energy. Next, the CEM was integrated with the TENG to improve its electrical output and drive the back-end function circuits to work effectively. Finally, the function circuits were designed to achieve water level information detection and signal transmission, together with the TENG and the CEM to form a self-powered intelligent buoy. This buoy is powered by the water wave energy in its working environment, and realizes information detecting and risk alarming of the working environment, constituting a complete self-powered and closed-loop system.

The structural design of the TENG device for harvesting water wave energy draws on our previous works.[36–39] In these papers, the advantage of the introduction of spring structures has been proven, which can store the elastic potential energy for continuous vibrations after mechanical triggering. In this work, we directly fabricated spiral TENG units with a spring-like shape instead of the combination of additional springs with TENGs, as shown in the right part of Figure 1c. For the promotion of industrialization, the availability of the materials utilized to prepare the TENG device was considered. Taking advantages of the flexibility and easy processing of the silica gel material, it was employed as the substrate of the TENG unit, and formed into a flat spring shape by 3D-printing technology. The diameter of the silica gel substrate is 35 mm with a layer thickness of 3 mm, and its height is 45 mm with the spring turns of 4. The stiffness coefficient of the silica gel substrate was tested as 630 N m^{-1}. The entire TENG unit was made by adhering copper foils on both sides of the substrate as electrodes, and bonding a 20 μm thick polyethylene terephthalate (PET) film on the electrode of one side as the dielectric layer, which can work in the contact-separation mode. The working principle of the spiral TENG unit is shown in Figure S1, Supporting Information. Under the action of external forces, the spiral TENG unit is compressed and elongated, so the electrode and the dielectric layer contact and separate accordingly, causing the accumulation of opposite charges on their respective surfaces. During the movement, the change of potentials between the two electrodes drives free electrons to flow through the external circuit, realizing the conversion from mechanical energy to electrical energy. This solution directly solves the difficulty of integrating the TENG units with ordinary spring elements, so the space structure and utilization are effectively improved. Then, considering the randomness of the wave conditions in the water hazard environment and the mechanism of water wave energy conversion, four spiral TENG units were arranged in the form of a regular tetrahedron inside an acrylic spherical shell with a diameter of 10 cm, which is described in the left part of Figure 1c. A copper ball was set at the center of the tetrahedron, ensuring sensibility of the whole spherical TENG. Under the triggering of water waves in any direction, the mass ball has relative motions with the spherical shell and drives the spiral TENG units to vibrate and output electrical signals. This design can accommodate water wave energy harvesting in different directions, improving the structure flexibility and energy conversion efficiency. In this way, the spherical TENG device that can collect water wave energy without the restrictions of orientations was organized.

Driven by the linear motor, the output performances of a single spiral TENG were evaluated at the frequency of 1.6 Hz, as shown in Figure S2, Supporting Information. The output current, output voltage, and transferred charge respectively reach 4.0 μA, 109.0 V, and 38.5 nC, which is not capable to satisfy the energy requirements of the functional circuits. In order to improve the output performances of the spiral TENG units, a CEM was designed in this work, which had been optimized based on our previous work.[40] The working principle of the CEM is illustrated in Figure 1d, which is to accumulate charges generated by the TENG and output electrical energy through series-parallel switching. The TENG unit in the left part works as the charge source for the entire CEM and drives all electronic elements in it. Here, the CEM is applied for the TENG unit at the contact-separation mode. Actually, the CEM is also suitable for TENGs in other working modes. In the middle part, the capacitor group contains two 47 μF capacitors, which are connected by diodes and two n-type metal-oxide-semiconductor field-effect transistors (MOSFETs). The switching of the MOSFETs is controlled by the alternating circuit (AC) output of the TENG, which is the energy source for the MOSFETs. As the TENG unit is compressed and stretched, the connection manner of the capacitor group switches between series and parallel periodically, leading to constant variation of the overall

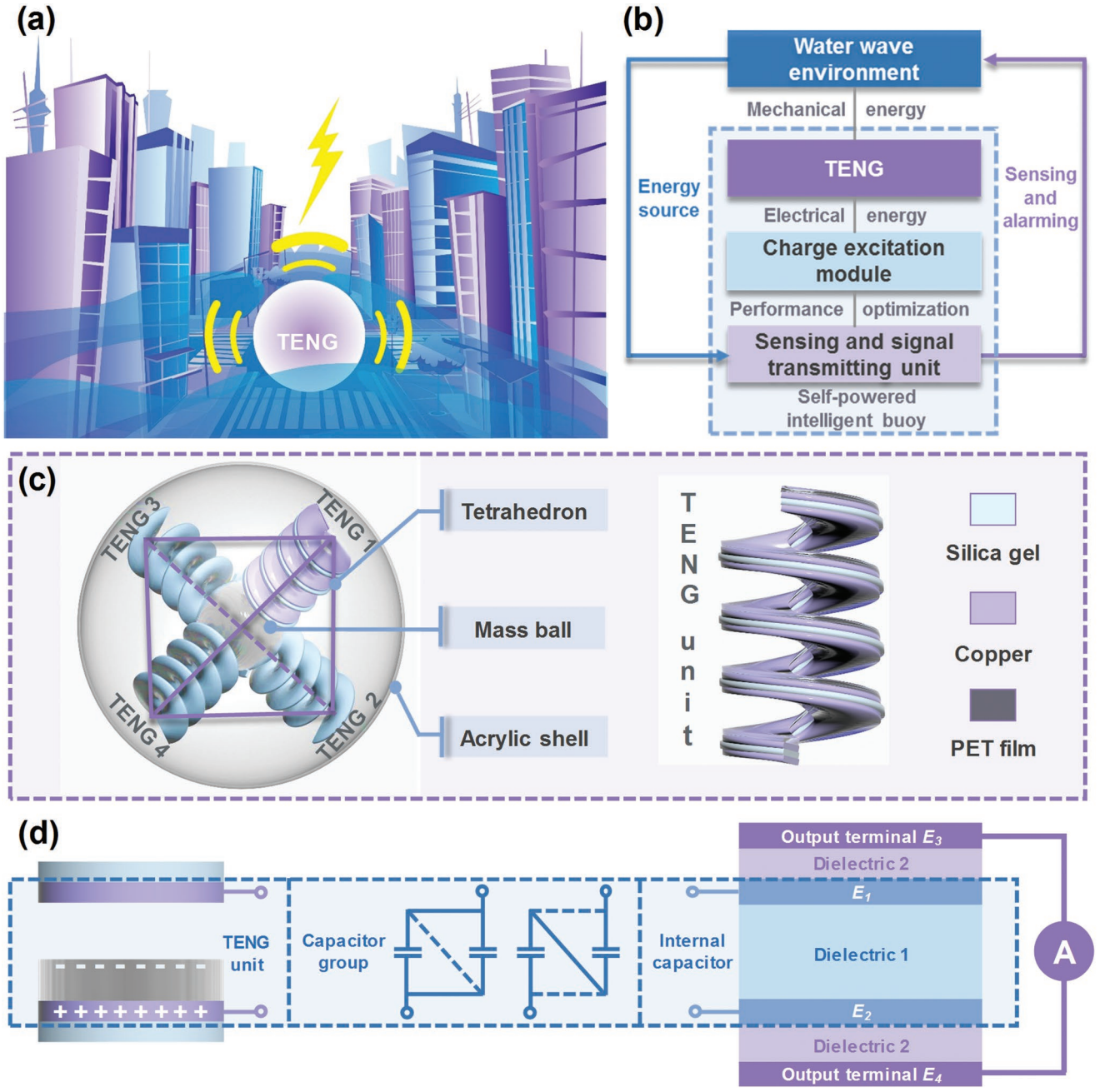

Figure 1. a) Schematic illustration of a self-powered water hazard alarming system using an intelligent TENG-based buoy through the water wave energy harvesting. b) Framework of the self-powered intelligent buoy for the water level is alarming. c) Structure of the spherical TENG and enlarged view of one spiral TENG unit inside. d) Schematic diagram of a contact-separation TENG integrated with the CEM.

voltage of the capacitor group. In the right part of Figure 1, the internal capacitor is constituted by Dielectric 1 and Electrodes E_1 and E_2. Here, Dielectric 1 is a round Kapton film with a diameter of 20 mm and a thickness of 0.1 mm, and the electrodes are made of aluminum. The capacitance of the internal capacitor is 0.05 nF, which is much smaller than that of the capacitor group. Therefore, the voltage change on the internal capacitor always follows the capacitor group, making charges flow back and forth between the capacitor group and the internal capacitor. For the purpose of confining the charges to the capacitor group and the inner capacitor, the output terminal was not set between them, avoiding these charges from flowing in the external circuit. In this CEM, two aluminum electrodes E_3 and E_4, serving as the output terminals, were integrated with the internal capacitor through Dielectric 2. The photograph of the internal capacitor and output terminals is exhibited in Figure S3, Supporting Information. The material of Dielectric 2 adopts lead zirconate titanate piezoelectric ceramics, with a relative permittivity of up to 3200. The shape of Dielectric 2 is a disc with a diameter of 20 mm and a thickness of 0.2 mm, so

the capacitance between E_1 and E_3 (E_2 and E_4) reaches 36 nF. When the voltage of the internal capacitor varies, the induced charges on E_3 and E_4 change accordingly, creating alternating charge flow in the external circuit. Note that E_1 and E_2 not only serve as the electrodes for the internal capacitor, but also forms capacitors with E_3 and E_4. Since ordinary commercial capacitors are impossible to achieve this configuration, the internal capacitor cannot be replaced by an ordinary commercial capacitor. The detailed circuit diagram of the CEM is shown in Figure S4, Supporting Information.

Due to the large capacitance of the capacitor group, the TENG cannot charge it to a high voltage in a limited time. For convenient, the state when the capacitors in the group are both charged to 6 V was discussed as a reference to describe the working principle of the CEM. In this case, the voltage curves of C_i (the internal capacitor), C_A (the capacitor between E_1 and E_3) and C_B (the capacitor between E_2 and E_4) are compared in **Figure 2**b. As the connection manner of capacitor group is switched between parallel and series by the TENG, its overall voltage varies between 6.0 and 12.0 V. Since the capacitance of the capacitor group is much larger than C_i, the voltage on C_i always keeps consistent with the capacitor group. In addition, the voltage on C_i is also equal to the sum of the voltages on C_A and C_B due to the short-circuit connection of E_3 and E_4 in the external circuit. Therefore, all voltage curves in Figure 2b vary regularly between high levels and low levels in the working process. When the voltage profiles reach high levels, the voltage on C_i is 12.0 V, while the other two are both 6.0 V, as marked in Figure 2b. The corresponding schematic diagram of charge distribution on electrodes E_1, E_2, E_3, and E_4 is demonstrated in the left part of Figure 2a. In order to maintain charge conservation and equipotentiality of E_3 and E_4, a certain amount of opposite charges are induced on the surfaces of E_3 and E_4. In the other situation marked with the cyan frame in Figure 2b, the voltage curves on C_i, C_A, and C_B decline to low levels, which are 6.0, 3.0, and 3.0 V, respectively. The voltage drop on C_i causes the induced charges on E_3 and E_4 to decrease, as shown in the right part of Figure 2a. The alternating increase and decrease of the induced charges lead to the charge flow through the external circuit. Driven by the linear motor, the output performances of the spiral TENG integrated with the CEM at the frequency of 1.6 Hz are shown in Figure S5, Supporting Information. The output current and transferred charge amount are separately improved to 60.4 μA and 94.4 nC, while the peak value of the output voltage is stable at 6.0 V. The results show that the integration of the CEM can not only regularize the electrical signals of the TENG, but also increase its output performances.

In order to further improve the transferred charges, two 1 μF capacitors were integrated with C_A and C_B in parallel, and the capacitances of the capacitor group were also increased to 1 mF. Figure 2c reveals the connection of a TENG unit and a CEM. The output current and the transferred charge curves of the TENG unit before and after being connected with the CEM are compared in Figure 2d,e. All tests were performed by the linear motor with the same parameters as above. The output current of the TENG unit is significantly improved from 4.0 μA to 4.3 mA, and the transferred charge is improved from 38.5 nC to 2.9 μC simultaneously, which is 74.3 times higher than before. The transferred charge density of the TENG reaches 1.36 mC m^{-3}, which is much better than that in previous work.[31] Because of the alternating characteristic of the output electrical signals, the rectification must be considered in the integration of the four spiral TENG units, and the connection diagram of a TENG unit, a CEM, and a rectifier bridge is shown in Figure 2f. Only the AC output of the TENG unit can control the normal operation of the CEM. If the TENG units are first connected with each other through the rectified bridges, the DC output converted will damage the electronic components inside the CEM. Therefore, the four TENG units are first connected to the CEMs and then to the rectified bridges, and the detailed circuit diagram of connecting the four TENG units in parallel is depicted in Figure S6a, Supporting Information. With increasing the unit number from one to four, the overall output currents of the TENG units in parallel are summarized in Figure 2g. The output current of four TENG units is 3.5 times of a single TENG unit, proving that the output current can be superimposed by paralleling several units. On the other hand, the overall output voltages of TENGs connected in series with different unit numbers are shown in Figure 2i, and the detailed circuit diagram is described in Figure S6b, Supporting Information. Similarly, the output voltage increases with the number of the TENG units, eventually demonstrating a 1.9 times improvement. These results illustrate that the CEM is provided with excellent integration performance. Furthermore, the output voltage of four TENG units in parallel and the output current of four TENG units in series are exhibited in Figure S7, Supporting Information. The results show the parallel connection cannot change the output voltage, while the series connection cannot change the output current, which is consistent with the general circuit logic.

For the purpose of harvesting water wave energy without the restriction of orientations, the four TENG units were arranged in the form of a regular tetrahedron inside a spherical shell with a copper mass ball at its center. This mass ball is the key to affect the working effect of the entire spherical TENG, so the structural optimization was conducted by changing the weight of the mass ball. Here, all spiral TENG units were directly connected in parallel by rectifier bridges without the CEMs for brevity. A free platform with six motors in various directions was applied to simulate water waves, and the wave frequency and height were fixed at 1.2 Hz and 10.6 cm. In **Figure 3**a–c, as the mass ball weight increases from 10 to 120 g, the output current, voltage, and power all first rise and then fall. The former uptrend is because the heavier mass ball exerts more force on the TENG units, while the overweight mass ball results in the subsequent drop due to its large inertia. When adopting the optimal weight of 60 g, the output current and voltage reach the maximum values of 60.4 μA and 414.0 V, respectively, and the maximum output power is 4.93 mW at the matched resistance of 4.7 MΩ.

After the structural optimization, a self-powered buoy was fabricated by integrating the four spiral TENG units, the CEMs, and rectifier bridges together. The photograph of the buoy is exhibited in Figure S8, Supporting Information, and the circuit diagram is indicated in Figure 3d. The diameter of the spherical buoy is 16 cm, with a weight of 488 g. The whole buoy only leads out one output terminal, simplifying the complexity of system wiring. The output performances of the buoy were measured under the water waves simulated by the six degrees of freedom platform, adjusting the wave conditions to

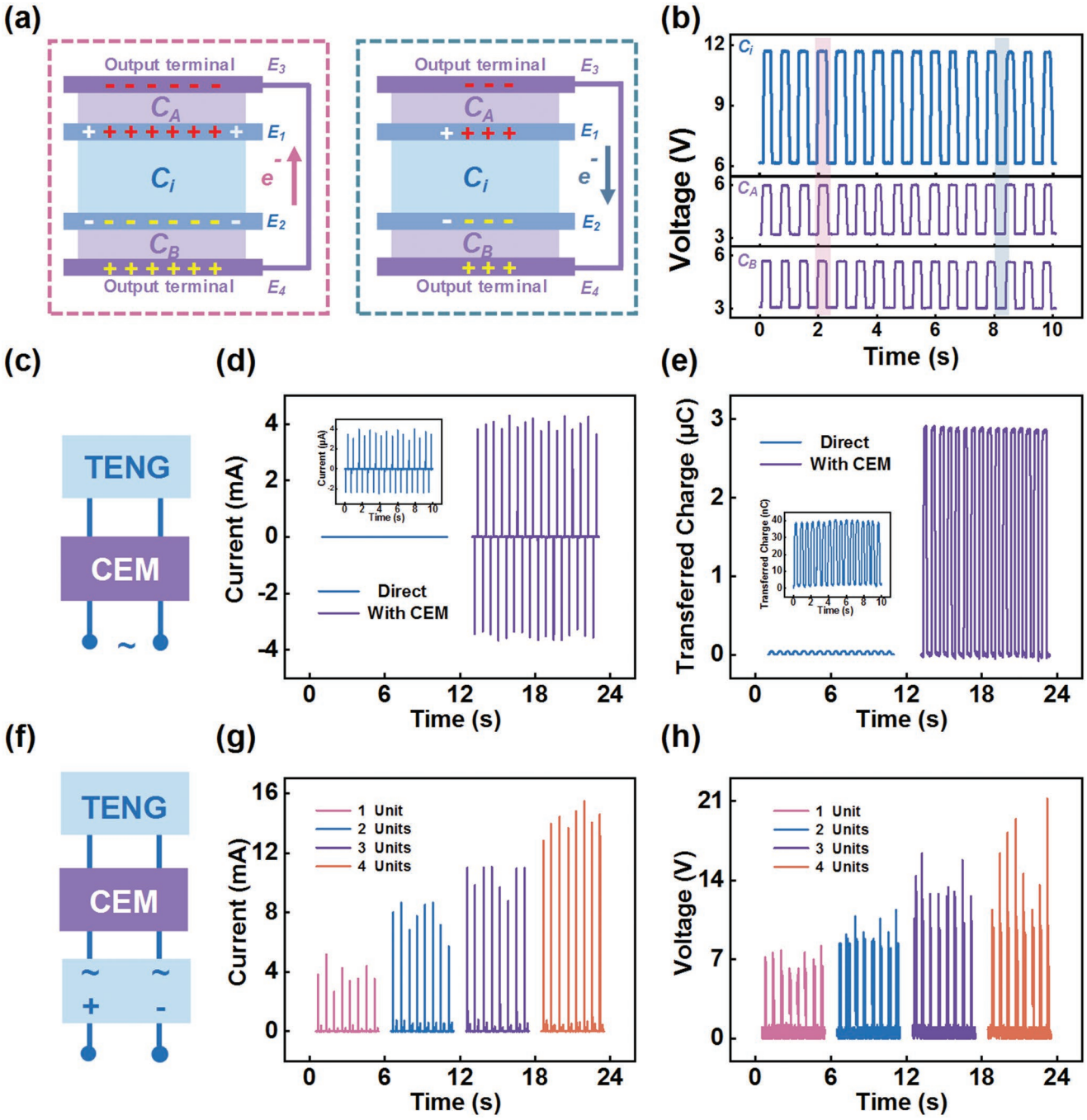

Figure 2. a) Schematic working principle of the CEM. b) Voltage change profiles on the capacitors C_i, C_A, and C_B in the CEM. c) Schematic diagram of a TENG unit integrated with a CEM. d,e) Comparison of (d) the output currents and (e) the transferred charges of one TENG unit before and after being connected with the CEM. f) Schematic diagram of a TENG unit integrated with a CEM and a rectified bridge. g) Overall output currents in parallel and (h) overall output voltages in series of the TENG units connected through the CEMs and rectified bridges as the number of units increases from 1 to 4.

be identical as before. Figure 3e illustrates the output current and output power as functions of the resistance. With the load resistance increasing from 10 Ω to 20 kΩ, the current decreases from 15.09 to 0.10 mA, while the power reaches the maximum value of 24.48 mW at the matched resistance of 680 Ω. Simultaneously, the power density of the buoy is calculated as 11.4 W m^{-3}. Note that the integration of the CEMs makes the matched resistance decrease from 4.7 MΩ to 680 Ω. The drop of the matched resistance breaks the restriction of the high equivalent internal impedance of the TENG and the unbalanced load match with the application circuits. The high equivalent internal impedance is ascribed to the low capacitance of the TENG. Here, the integration of the CEM greatly increases the capacitance of the TENG, and its equivalent internal impedance declines accordingly. Thus, the matched resistance for the output power reduces obviously. In Figure 3f, the short-circuit

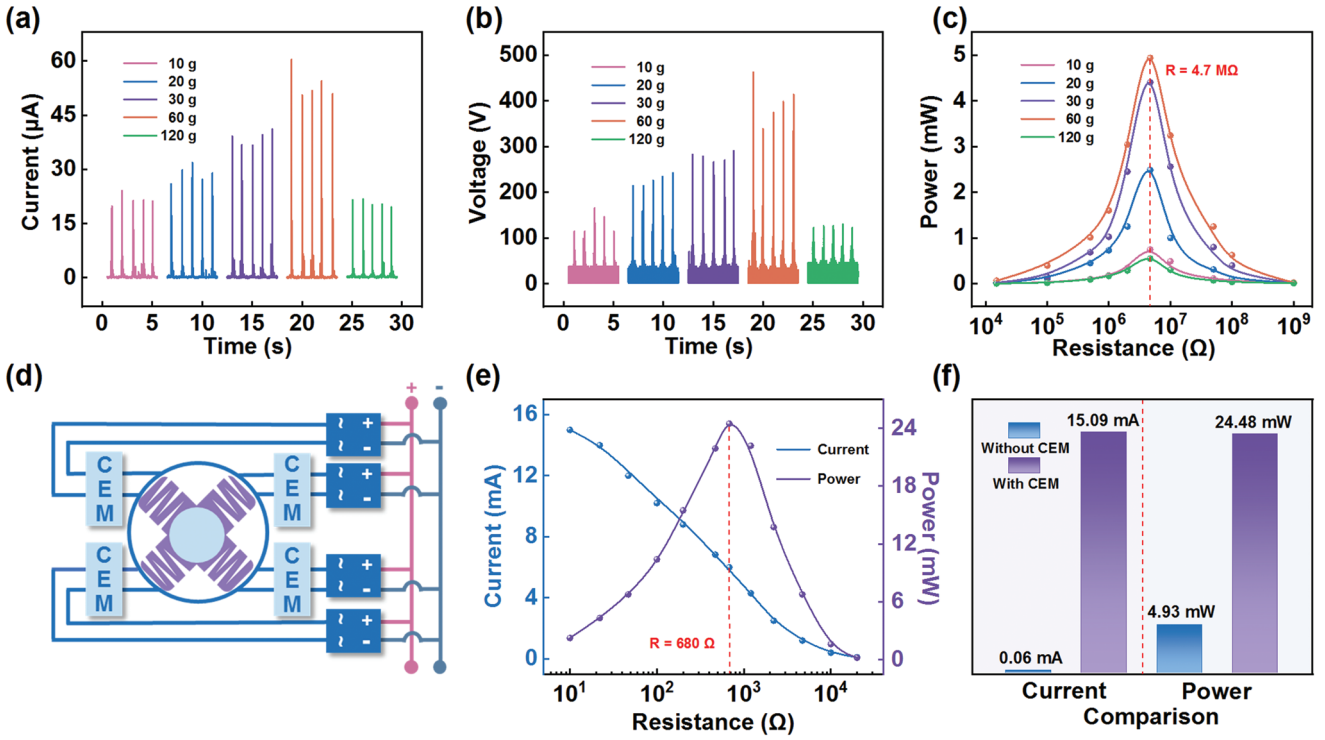

Figure 3. a) Output currents, b) output voltages, and c) output power-resistance profiles of the spherical TENG for various weights of mass ball. d) Schematic diagram of the parallel connection of the spiral TENG units inside the spherical structure through the CEMs and rectified bridges. e) Output current and output power with respect to the load resistance for the spherical TENG integrated with the CEMs. f) Comparison of the output current and the output power of the spherical TENG with or without the CEMs.

current and maximum power are compared with the results before connecting with the CEMs. It can be found that the current and power are improved by 250.5 times and 4.0 times, respectively, verifying the working effect of the CEMs obviously.

Subsequently, the influences of the water wave frequency and height on the output performances of the buoy were investigated. By adjusting the motion parameters of the free platform, various water wave conditions were simulated to trigger the buoy to work. The output current and output voltage for the buoy under different wave frequencies are shown in **Figure 4**a,b at the fixed wave height of 10.6 cm. As the wave frequency increases from 0.7 to 2.2 Hz, the peak values of the output current and output voltage all first increase and then decrease, exhibiting the maximum values of 15.1 mA and 16.0 V at the frequency of 1.2 Hz. The initial increase of the output current is due to the higher voltage inputting into the CEM. However, excessive triggering frequency results in a large switching loss of the MOSFETs in the CEM, so the output current is not in a monotony increasing trend with the frequency. In Figure 4c, the power-resistance relationships under different wave frequencies present the similar tendency, and the maximum value of 24.48 mW is also obtained at the frequency of 1.2 Hz. However, the matched resistance decreases from 1.2 kΩ to 680 Ω with increasing the wave frequency. On the other hand, the output characteristics of the buoy under different wave heights were also studied when fixing the wave frequency at 1.2 Hz, as shown in Figure 4d–f. The output current, output voltage, and output power are all enhanced with higher waves, implying the larger wave height is beneficial for the buoy to work efficiently. The relatively lower output performances at smaller wave heights are ascribed to its own weight of the buoy, which is difficult to be driven by slighter water waves. Afterward, setting the wave frequency at 4 Hz and the wave height at 10.6 cm, the average power of the buoy under different resistances was studied, as shown in Figure S9, Supporting Information. It can be found that the buoy can produce a maximum average power of 0.86 mW at the matched resistance of 680 kΩ. Although the peak values of the output current decrease with the increasing load resistances, the width of the current peaks becomes significantly broader, resulting in the higher matched resistance of the average power.

Considering the special purpose of this buoy for water hazard alarming, we simulated the submergence of a city in Yellow River Basin when it suffers a 20 year flood by means of the FLO-2D software. Figure 4g displays the simulation map of the submerged water level situation. The simulation results indicate the maximum and minimum water depths are 3.37 and 0.20 m, respectively, and the average value is 0.33 m. According to the average water depth and the local average wind speed, the water wave frequency and height can be calculated as 1.25 Hz and 3.2 cm (Note S1, Supporting Information). Because the buoy was pieced together from two hemispheres, all seams were tightly sealed with tile cement to prevent water leakage and penetration. As for the output leads, special waterproof plugs were applied to realize great waterproof performance. After the sealing and waterproofing process, the buoy

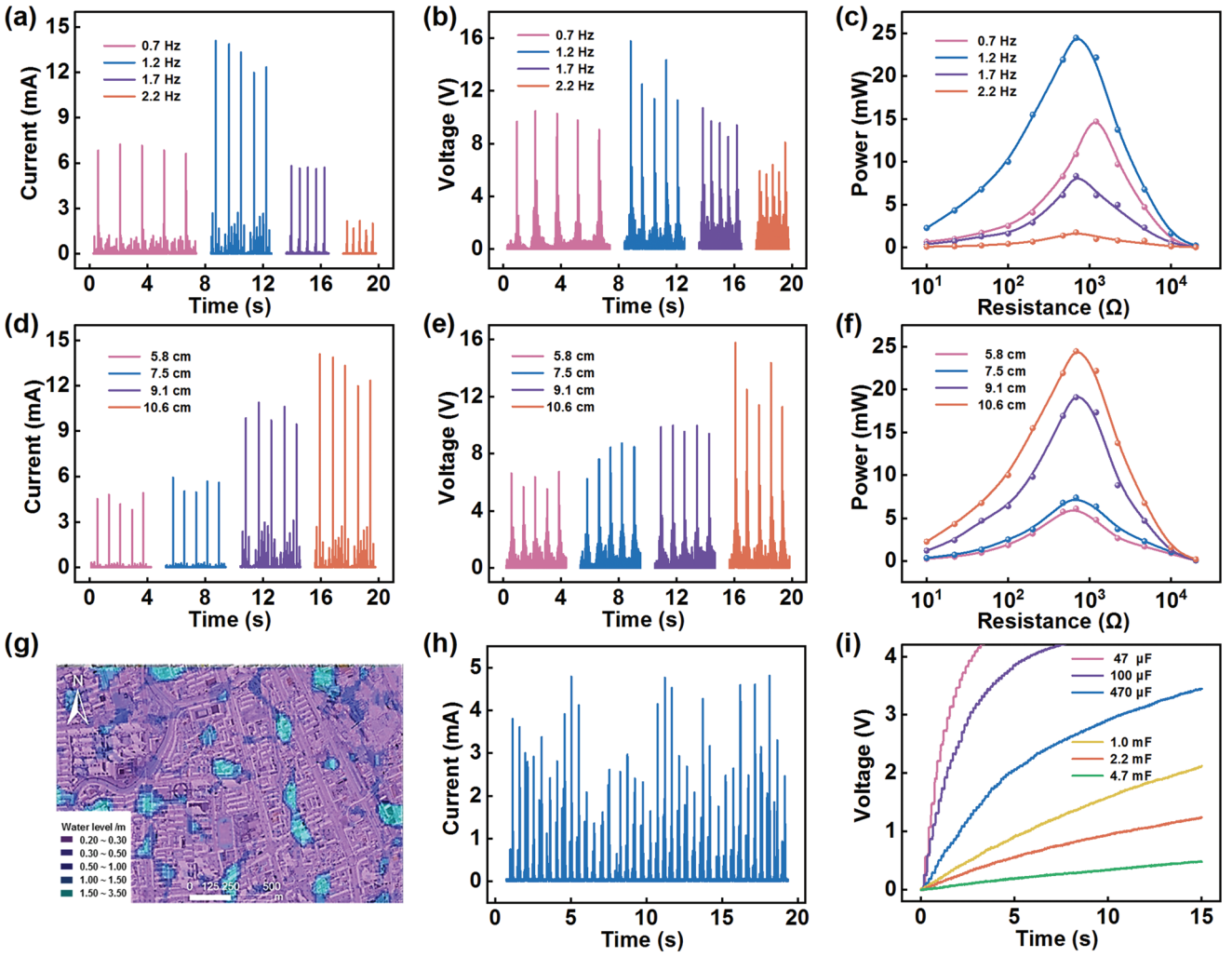

Figure 4. a) Output currents, b) output voltages, and c) output power-resistance profiles of the spherical TENG integrated with the CEMs at various water wave frequencies. d) Output currents, e) output voltages, and f) output power-resistance profiles of the spherical TENG integrated with the CEMs at various water wave heights. g) Simulation map of the submerged water level situation of a city in the Yellow River Basin that suffers a 20 year flood. h) Output current of the spherical TENG integrated with the CEMs under the simulated flood wave conditions. i) Charging voltage curves to various capacitors for the spherical TENG integrated with the CEMs.

was placed in a water tank with the water depth of 0.33 m. A series of wave pumps were applied to generate water waves consistent with the simulation results. In Figure 4h, the output current of the buoy in the water environment was measured, and the maximum peak current reaches 4.8 mA. Moreover, the capabilities of the buoy for charging different capacitors were also investigated, as presented in Figure 4i. The voltage on the 470 μF capacitor can be raised from 0 to 3.44 V within 15 s by the buoy under the water waves. For comparison, the voltage profile of the spherical TENG without CEMs for charging the 470 μF capacitor is also exhibited in Figure S10, Supporting Information, and the single spherical TENG can only charge the capacitor to 0.03 V within the same charging time. The charging speed of the TENG with the CEMs is 113 times faster than that of direct charging, illustrating the distinctly positive effect of the CEMs on the charging performance of the TENG. The significant improvement is due to the increased transferred charge per working cycle for the charge excitation TENG.

Based on the powerful wave energy harvesting capability of the TENG, a self-powered water level alarm system was developed. **Figure 5**a shows the schematic diagram of the transmitting terminal powered by the spherical TENG integrated with the CEMs. Firstly, the TENG units inside the spherical structure were connected in parallel through the CEMs and rectifier bridges. Then, a 470 μF capacitor was applied to store electrical energy to power the function circuit, which includes the water level sensor unit and the signal transmitting unit. Here, the water level sensor unit is a switch that can sense the change in the water level, which can be automatically switched when the water level reaches a certain set value. The signal transmitting unit can transmit radio frequency signals with the frequency of 433 MHz. The spherical TENG, the CEMs, the rectifier bridges, the capacitor, and the signal transmitting unit were integrated together to constitute a self-powered intelligent buoy. However, in order to guarantee the accuracy of the water level alarm system, the water level sensor unit was placed on the

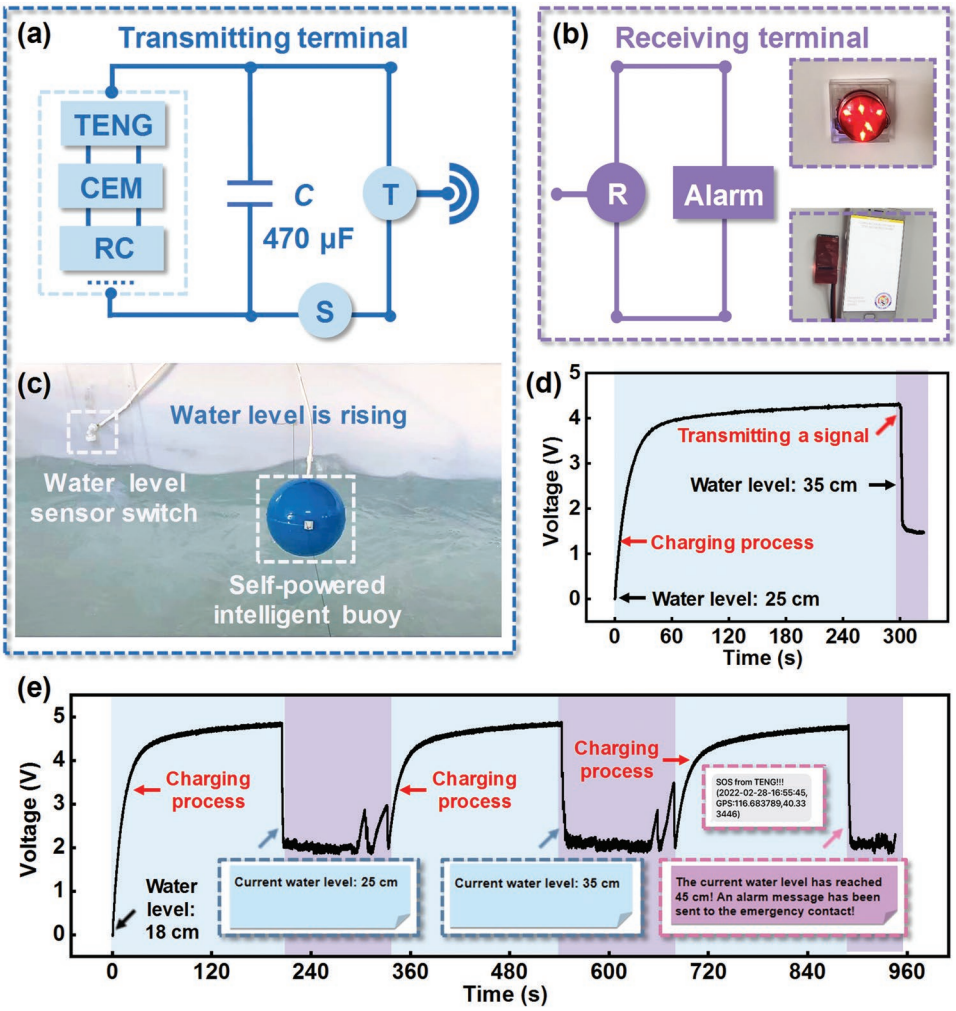

Figure 5. a) Schematic diagram of the transmitting terminal powered by the spherical TENG integrated with the CEMs. b) Circuit diagram of the receiving terminal and photographs of an LED indicator and a mobile phone. c) Photographs of the water wave environment and the self-powered intelligent buoy placed in it. d) Voltage curve on the transmitting terminal of the water level alarm system. e) Voltage curve on the transmitting terminal of the water level information exchange system.

inner wall of the water tank instead of the interior space of the buoy. Figure 5c shows the photograph of the complete transmitting terminal and the water wave environment in which it works. On the other hand, the circuit diagram of the receiving terminal and the photographs of an LED indicator and a mobile phone for alarming are exhibited in Figure 5b. For considering the experimental space constraints, the receiver terminal was set at a distance of 25 m away from the transmitting terminal. However, theoretically, the transmitting distance can reach 50 m.

Utilizing the LED indicator, a simple water level alarm system was constructed, and the voltage curve on the transmitting terminal in the working process is shown in Figure 5d. The initial water level was 25 cm, while the water level sensor switch was set at 35 cm. As the water level continues to rise, the spherical TENG is triggered by the water waves to convert the mechanical energy to electrical energy and store it in the capacitor, which corresponds to the charging process in Figure 5d. The precharging time is 20 s. After the precharging time of 20 s, the voltage of the transmitting terminal can be charged to 3 V, which is the voltage that the transmitter needs to start work. When the water level reaches 35 cm, the water level sensor switch is turned on and the signal transmitting unit works. In this way, the receiving terminal receives the signals and the LED indicator is lit up. The demonstration of the water level alarm system can be found in Video S1, Supporting Information.

Furthermore, a water level information exchange system between the self-powered intelligent buoy and a mobile phone was constructed. The detailed circuit diagram of the transmitting terminal is depicted in Figure S11, Supporting Information, and its voltage curve during the working process is shown in Figure 5e. The water level sensor unit contains three sets of sensor switches, which are respectively set at the water level of 25, 35, and 45 cm. Although the pre-charging time is relatively short, the setting distance of the sensor switches can be hardly reduced because of the limited sensing accuracy. Note that S_1, S_3, and S_5 are normally closed switches, while S_2 and S_4 are normally open switches. As the water level starts to rise from 18 cm, the spherical TENG continues to charge the

capacitor and makes the voltage raised. When the water level reaches 25 cm, S_1 is turned on and the water level information is transmitted to the mobile phone. The insert of Figure 5e shows the information displayed on the mobile phone screen. In the next period, S_1 and S_2 keep opening or closing due to the unstable water level, so the voltage curve remains vibrating. The charging process restarts until S_1 and S_2 achieve steady on and off states, respectively. The voltage curves during the period of the water level rising to 35 and 45 cm are similar as before. When the water level exceeds 45 cm, there is a risk of water overflowing. After the mobile phone receives this information, it automatically makes a phone call and sends a text message containing the GPS information to the emergency contact. The experimental process was recorded in Video S2, Supporting Information.

3. Conclusion

In this work, a self-powered intelligent buoy based on the TENG energy harvester was constructed for water hazard alarming system via water wave energy conversion. For improving the output performance, the CEMs were designed and integrated inside the buoy. Under the optimal water wave condition, the maximum output current and output power of the spherical TENG with CEMs reach 15.09 mA and 24.48 mW, respectively. Utilizing the high electrical outputs, the water level alarm system and the water level information exchange system with a mobile phone were successfully demonstrated. This self-powered intelligent buoy realizes functional applications by collecting water wave energy in its working environment, breaking the limitation of the commercial electricity. This work not only broadens the application range of the TENG toward water wave energy harvesting and provides an experimental basis for the development of the IoTs, but also comes up with new ideas for disaster prevention, which even contributes to the carbon neutralization.

4. Experimental Section

Fabrication of the Spherical TENG: First, four spiral TENG units inside the spherical structure were fabricated. The substrates of the TENG units were flat springs of silica gel, shaped by the 3D-printing technology. The diameter of the substrate was 35 mm with the layer thickness of 3 mm, and the height is 45 mm with the spring turns of 4. Then, copper foils were attached to both sides of the substrate as electrodes, and a 20 µm thick PET film was bonded with an electrode on one side as the dielectric layer. Finally, four spiral TENG units were integrated as a regular tetrahedron in an acrylic spherical shell with a diameter of 10 cm, and a copper ball was placed at the center of the tetrahedron, forming a complete spherical TENG.

Fabrication of the Self-Powered Intelligent Buoy: The spherical TENG, CEMs, rectifier bridges, and signal transmitting units were connected together in a polypropylene (PP) spherical shell with a diameter of 16 cm. Almost all the wires were arranged inside the shell, except two wires which were led out as the output terminals. After the shell was waterproofed by the tile cement, the self-powered intelligent buoy was fabricated.

Electric Measurements of the TENG Device: The electric outputs of the spiral TENG units were measured under regular triggering provided by the linear motor (LINMOT 1100). A platform with 6° of freedom was applied to simulate water wave motions to drive the TENG device. A series of wave pumps (YHX 021) was set at the inner walls of a water tank to construct real water wave environment. The output current, output voltage, and transferred charge of the TENG device were measured by a current preamplifier (Keithley 6514 System Electrometer), while the voltage after rectification was measured by a digital oscilloscope (Agilent InfiniiVision 2000X).

Supporting Information

Supporting Information is available from the Wiley Online Library or from the author.

Acknowledgements

X.L. and S.L. contributed equally to this work. Support from the National Key R & D Project from the Minister of Science and Technology (2021YFA1201603, 2021YFA1201601), National Natural Science Foundation of China (Grant Nos. 51432005, 51702018, and 51561145021), and the Youth Innovation Promotion Association, CAS, were appreciated. The authors also thank Hairong Long, Kai Han, Hao Pang, and Jiajia Han for device fabrications and measurements.

Conflict of Interest

The authors declare no conflict of interest.

Data Availability Statement

The data that support the findings of this study are available from the corresponding author upon reasonable request.

Keywords

charge excitation modules, self-powered systems, triboelectric nanogenerators, water hazard alarming, water wave energy harvesting

Received: May 10, 2022
Revised: June 6, 2022
Published online:

[1] B. Tellman, J. A. Sullivan, C. Kuhn, A. J. Kettner, C. S. Doyle, G. R. Brakenridge, T. A. Erickson, D. A. Slayback, *Nature* **2021**, *596*, 80.
[2] H. Shiogama, M. Watanabe, H. Kim, N. Hirota, *Nature* **2022**, *602*, 612.
[3] M. Kotz, A. Levermann, L. Wenz, *Nature* **2022**, *601*, 223.
[4] Y. M. Won, J. H. Lee, H. T. Moon, Y. I. Moon, *Water* **2022**, *14*, 187.
[5] A. Fekete, S. Sandholz, *Water* **2021**, *13*, 3016.
[6] M. E. Idrissi, O. E. Beqqali, J. Riffi, *Arabian J. Geosci.* **2021**, *14*, 2109.
[7] F. R. Fan, Z. Q. Tian, Z. L. Wang, *Nano Energy* **2012**, *1*, 328.
[8] Z. L. Wang, *Mater. Today* **2017**, *20*, 74.
[9] Z. L. Wang, *Rep. Prog. Phys.* **2021**, *84*, 096502.
[10] X. S. Zhang, M. D. Han, B. Meng, H. X. Zhang, *Nano Energy* **2015**, *11*, 304.
[11] Z. Ren, Z. Wang, Z. Liu, L. Wang, H. Guo, L. Li, S. Li, X. Chen, W. Tang, Z. L. Wang, *Adv. Energy Mater.* **2020**, *10*, 2001770.

[12] H. Wu, S. Wang, Z. Wang, Y. Zi, *Nat. Commun.* **2021**, *12*, 5470.
[13] W. He, W. Liu, J. Chen, Z. Wang, Y. Liu, X. Pu, H. Yang, Q. Tang, H. Yang, H. Guo, C. Hu, *Nat. Commun.* **2020**, *11*, 4277.
[14] Y. Li, Z. Zhao, L. Liu, L. Zhou, D. Liu, S. Li, S. Chen, Y. Dai, J. Wang, Z. L. Wang, *Adv. Energy Mater.* **2021**, *11*, 2100050.
[15] X. Wang, S. Niu, Y. Yin, F. Yi, Z. You, Z. L. Wang, *Adv. Energy Mater.* **2015**, *5*, 1501467.
[16] C. Hou, T. Chen, Y. Li, M. Huang, Q. Shi, H. Liu, L. Sun, C. Lee, *Nano Energy* **2019**, *63*, 103871.
[17] X. S. Zhang, M. D. Han, R. X. Wang, F. Y. Zhu, Z. H. Li, W. Wang, H. X. Zhang, *Nano Lett.* **2013**, *13*, 1168.
[18] Z. L. Wang, *Faraday Discuss.* **2014**, *176*, 447.
[19] Z. L. Wang, *Adv. Energy Mater.* **2020**, *10*, 2000137.
[20] Z. L. Wang, J. Chen, L. Lin, *Energy Environ. Sci.* **2015**, *8*, 2250.
[21] C. Rodrigues, D. Nunes, D. Clemente, N. Mathias, J. M. Correia, P. R. Santos, F. T. Pinto, T. Morais, A. Pereira, J. Ventura, *Energy Environ. Sci.* **2020**, *13*, 2657.
[22] Z. L. Wang, *Nature* **2017**, *542*, 159.
[23] Z. L. Wang, T. Jiang, L. Xu, *Nano Energy* **2017**, *39*, 9.
[24] Q. Shi, H. Wang, H. Wu, C. Lee, *Nano Energy* **2017**, *40*, 203.
[25] X. Wei, Z. Zhao, C. Zhang, W. Yuan, Z. Wu, J. Wang, Z. L. Wang, *ACS Nano* **2021**, *15*, 13200.
[26] H. Pang, Y. Feng, J. An, P. Chen, J. Han, T. Jiang, Z. L. Wang, *Adv. Funct. Mater.* **2021**, *31*, 2106398.
[27] Y. Feng, X. Liang, J. An, T. Jiang, Z. L. Wang, *Nano Energy* **2021**, *81*, 105625.
[28] Q. Zhang, L. Li, T. Wang, Y. Jiang, Y. Tian, T. Jin, T. Yue, C. Lee, *Nano Energy* **2021**, *90*, 106501.
[29] J. Zhu, H. Wang, Z. Zhang, Z. Ren, Q. Shi, W. Liu, C. Lee, *Nano Energy* **2020**, *73*, 104760.
[30] L. Liu, Q. Shi, J. S. Ho, C. Lee, *Nano Enegy* **2019**, *66*, 104167.
[31] F. Xi, Y. Pang, G. Liu, S. Wang, W. Li, C. Zhang, Z. L. Wang, *Nano Energy* **2019**, *61*, 1.
[32] Z. Wu, H. Guo, W. Ding, Y. C. Wang, L. Zhang, Z. L. Wang, *ACS Nano* **2019**, *13*, 2349.
[33] H. Wang, Q. Zhu, Z. Ding, Z. Li, H. Zheng, J. Fu, C. Diao, X. Zhang, J. Tian, Y. Zi, *Nano Energy* **2019**, *57*, 616.
[34] C. Zhang, L. Liu, L. Zhou, X. Yin, X. Wei, Y. Hu, Y. Liu, S. Chen, J. Wang, Z. L. Wang, *ACS Nano* **2020**, *14*, 7092.
[35] T. Zhao, M. Xu, X. Xiao, Y. Ma, Z. Li, Z. L. Wang, *Nano Energy* **2021**, *88*, 106199.
[36] T. Jiang, Y. Y. Yao, L. Xu, L. M. Zhang, T. X. Xiao, Z. L. Wang, *Nano Energy* **2017**, *31*, 560.
[37] X. Liang, Z. Liu, Y. Feng, J. Han, L. Li, J. An, P. Chen, T. Jiang, Z. L. Wang, *Nano Energy* **2021**, *83*, 105836.
[38] T. X. Xiao, X. Liang, T. Jiang, L. Xu, J. J. Shao, J. H. Nie, Y. Bai, W. Zhong, Z. L. Wang, *Adv. Funct. Mater.* **2018**, *28*, 1802634.
[39] T. X. Xiao, T. Jiang, J. X. Zhu, X. Liang, L. Xu, J. J. Shao, C. L. Zhang, J. Wang, Z. L. Wang, *ACS Appl. Mater. Interfaces* **2018**, *10*, 3616.
[40] X. Liang, T. Jiang, Y. W. Feng, P. J. Lu, J. An, Z. L. Wang, *Adv. Energy Mater.* **2020**, *10*, 2002123.